Supporting Information (SI)

For

Alginate Promotes Soil Phosphorus Solubilization Synergistically with Redox-Active Antibiotics through Fe(III) Reduction

Xinfei Ge,[a] Lijun Wang,[a] Xiong Yang,[a] Guohong Qiu,[a] and Wenjun Zhang[a,*]

[a]College of Resources and Environment, Huazhong Agricultural University, Wuhan 430070,

China

Number of pages: 19

Number of figures: 12

Number of tables: 3

SI Methods

Materials. Unless stated otherwise, all reagents including alginate of a high polymerization degree (H Alginate; n ≈ 500) were purchased from Sigma-Aldrich (St. Louis, Missouri). Additionally, alginates of middle (M Alginate; n ≈ 50, M/G > 4) and low (L Alginate; n = 5; M/G > 4) polymerization degrees were purchased from Elicityl Biotech Company. 1-hydroxyphenazine (1-OHPHZ), phenazine-1-carboxylic acid (PCA) and phenazine-1-carboxamide (PCN) in oxidized forms were all purchased from TCI America. The most studied model protein of bovine serum albumin (BSA; MW ≈ 66.5 kDa and pI ≈ 4.7) was obtained from Fluka (St. Louis, Missouri), and the typical supercoiled pBR322 DNA (4361 base pairs) was obtained from Takara Biomedical Technology (Beijing, China). All experimental solutions were prepared using ultrahigh purity water (18.2 MΩ·cm) obtained through a two-step purification treatment including a triple distillation (YaR, SZ-93, Shanghai, China) and deionization (Milli-Q, Billerica, MA).

Preparation of Iron(III) Phosphate Minerals and Reduced Phenazines. Amorphous iron(III) phosphate (AmFe(III)-P) with a solid Fe/P mole ratio of ≈ 1[1-3] was synthesized by mixing 150 mL iron(III) chloride (0.2 M) with 150 mL phosphoric acid (0.3 M) followed by adjusting pH to 3. The surfactants CTAB (hexadecyl trimethyl ammonium bromide) of 1.5 % of the mass of iron power was dissolved in 100 mL water contained 18.3 mL phosphoric acid (85%) and 5 g iron power. The solution was stirred at 60 °C until completely clarified followed by removing the insoluble black solid impurities. Next, H_2O_2 (82.5 mL, 5 %) was gradually added to the clear light green solution accompanied by occurrence of oxidation reaction at 70°C with a constant pH 2 using ammonia water adjustment. The obtained solution was stirred until the formation of a white slurry under the optimal conditions of 4 h aging time and 60 min ultrasonic time.[4] Both AmFe(III)-P and crystalline iron(III) phosphate (CryFe(III)-P) precipitates were filtered, washed with water and alcohol at least three times, respectively, to remove adsorbed iron and phosphate as much as possible and dried at 80 °C under vacuum for 12 h to obtain the final products. Those products were characterized by both X-ray

diffraction (XRD, Bruker D8, Billerica, MA) and Raman spectroscopy (Horiba LabRAM HR800) (Figure S1).

1-OHPHZ, PCA and PCN in their oxidized forms all were dissolved in high (100 mM KCl) or low (10 mM KCl) salt solutions, respectively, buffered with 10 mM (5 mM each) $CH_3C(O)ONH_4$-MOPS (3-(n-morpholino)propanesulfonic acid) to maintain constant pH yielding 100 or 200 mg/L PHZ-bearing solutions used for electrochemical experiments. The reduced form of each PHZ (H_2PHZ) was obtained through the quantitative two-electron transfer (Figure S2) with a controlled potential bulk electrolysis in a buffer solution at pH 7. Complete PHZ reduction was confirmed by linear sweep voltammetry (LSV) before and after the bulk electrolysis of each PHZ using the working electrode for cyclic voltammetry. The experimental details can be seen in a previous study.[5] In addition, H Alginate-bearing solutions with different concentrations of 100, 200 and 500 mg/L used for reduction dissolution were also prepared. The concentration of alginate and PHZ in natural soil systems have distinct variations in different geological environments or agricultural settings, whose ranges used in the present study frequently occurs in EPS-bearing soil microenvironments, especially in organics-rich soil. During electrochemical experiments, all solutions were deoxygenated and reactions were conducted under oxygen-free conditions with protection by nitrogen (N_2).

Batch Reduction Experiments. Unless specified otherwise, all batch reduction experiments were performed by adding 100 mg AmFe(III)-P or CryFe(III)-P into 15 mL of H_2PHZ-, H Alginate- or (H_2PHZ + H Alginate)-bearing buffer solutions with different pH values (4, 5, 7 and 8) and salt concentrations (high and low salt) at 25 °C under sterile and anoxic conditions with nitrogen (N_2) protection throughout the reaction in vacuum glove box. The control assays were also conducted only in buffer solution without H_2PHZ and H alginate to exclude the interference from adsorbed Fe/P and aqueous buffer solution. All reactions were initiated in the dark and immediately quenched after reaction for 30 min. Then, the reacted solutions were filtered through a 0.22 μm filter and the residual solid iron(III) phosphate was washed to collect the

filtrate containing dissolved Fe(II), Fe(III) and concomitantly released P. The obtained filtrates were then quickly centrifuged at 10000 r/min for 2 min using a 5810R bench freezing centrifuge (Eppendorf, Germany) to further remove the suspended iron(III) phosphate and avoid the (photo)oxidation of reduced Fe(II).

Determination of Reductive Dissolution Content of Fe(II). Prior to quantification of Fe(II) production with ferrozine (FZ) method,[6] the filtrates were adjusted to a neutral pH using a 0.1 M HCl or 0.1 M KOH stock solution, in which FZ can extremely rapidly and selectively react with Fe(II) rather than Fe(III)[7, 8] by the formation of a stable purple complex, Fe(II)FZ$_3$, with a maximum absorbance at 562 nm.[6, 9, 10] Then, the production of Fe(II) was quantified using a UV spectrophotometer (UV1800ENG240, Japan) equipped with a 1 cm path length cell after 30-60 s of reaction time (the time for full color development)[11] by adding 4 mL FZ (10 mM) solution into the collected filtrates, followed by dilution to a constant volume of 25 mL in colorimetric tube. Noticeably, the FZ concentration utilized in this study was sufficient for both free Fe(II) and organic-complexed Fe(II) quantifications,[12] which resulted in negligible free Fe(II), PHZ-Fe(II) or H alginate-Fe(II) complex even at high soil organic matter concentrations[13, 14] and the reason for choosing the mass of 100 mg iron(III) phosphate was that for the reductive dissolution of CryFe(III)-P, Fe production were above the detection limit of FZ method. Moreover, quick introduction of FZ solution can completely outcompete Fe(II) oxidation, which confirmed in a previous study.[15] Standing solution of Fe(II) ranging from 0 to 5000 µg/L were prepared and the detection limit was 2.5 µg/L.[16] Total Fe (Fe$_T$) content was quantified through the reduction of Fe(III) in filtrates to Fe(II) using hydroxylamine hydrochloride[17]and the Fe(III) content in each aliquot was calculated from the difference between measured Fe$_T$ and Fe(II).

One supplementary experiment was performed to explore the role of organic-complexed Fe(III) in enhancing solid-phase Fe(III) reduction by H$_2$PHZ. The prepared H alginate-Fe(III) complex (1 mM) and free Fe(III) ion (1 mM) were added into the H$_2$PHZ-bearing buffer solutions (200 mg/L; pH 5; high salt), respectively. The Fe(II) production from free or H alginate-complexed Fe(III) reduction by H$_2$PHZ was

determined by FZ method. Here, it should be noted that H alginate concentration was slightly higher than that of Fe(III) ion to ensure the complete complexation of Fe(III) by H alginate. Another possible reaction in the system is the solid-phase Fe(III) in iron(III) phosphate reduction by H alginate-Fe(II) complex acting as electron shuttle analogues. To verify this possibility, the oxygen-free H alginate-Fe(II) complex (1 mM) and free Fe(II) ion (1 mM) were prepared in buffer solutions (pH 5; high salt) followed by the addition of 100 mg iron(III) phosphates. The Fe(III) production from free or H alginate-complexed Fe(II) oxidization by solid-phase Fe(III) reduction was determined from the difference as measured Fe_T and Fe(II). Here, it should be noted that H alginate concentration was slightly lower than that of Fe(II) ion to avoid interference of excess H alginate dissolution for ion(III) phosphates.

Determination of P Production Content with Fe(III) Reduction. Additionally, the released P content accompanied by reductive dissolution of iron(III) phosphates was quantified by a molybdenum blue staining method.[18] a. Preparations of Color Reagents. Reagent A: sulfuric acid (5 N). Dilute 70 ml concentrated sulfuric acid (95-98%, GR) to 500 ml. Reagent B: ascorbic acid (0.1 M). Dissolve 1.32 g of ascorbic acid (MW 176.12, AR) in 75 ml of water. Because of easily oxidization, the solution should be prepared without light. Reagent C: ammonium molybdate (4 %). Dissolve 20 g ammonium molybdate (MW 1235.86, AR) in water and dilute to 500 ml. And store the solution in a brown bottle. Reagent D: potassium antimony tartrate (1 mg Sb/ml). Dissolve 0.2743 g of potassium antimony tartrate (MW 333.93, CP) in 100 ml of water. Reagent E: mixed reagent. The color reagent was prepared by mixing thoroughly 125 ml of 5 N sulfuric acid, 37.5 ml of ammonium molybdate, 75 ml of ascorbic acid and 12.5 ml of potassium antimony tartrate solution. b. Determination of P Standard Curve. Accurately weigh 0.4390 g of potassium dihydrogen phosphate (KH_2PO_4, Sigma-Aldrich) dried in an oven at 80 °C for 2 h. Dissolve it with water, add 5 ml of concentrated sulfuric acid and water to 1000 ml constant volume. Finally, the standard reserve solution containing 100 mg P/L was obtained. A series of standard solutions containing 0.0, 0.2, 0.6, 1.0, 2.0, 3.0, 4.0, 5.0 mg P/L were prepared by diluting the

standard reserve solution. All standard solutions were adjusted to neutral conditions using 2, 4-dinitrophenol indicator (MW 184.11, AR) by dropping 0.1 M HCl or 0.1 M KOH stock solution, respectively. Then, add 4 ml of color reagent and dilute to 25 ml in colorimetric tube. After 30 min at room temperature, the absorbance was measured by using UV spectrophotometer (UV1800ENG240, SOFT, SHIMADZU, Japan) at $\lambda =$ 880 nm.

c. Orthophosphate Determination. Before the quantification of P content, the blank measurement only with buffer solution was performed to eliminate the interference of adsorbed P and only minor impurities of P existed on iron(III) phosphates were detected within error. Thus, the concentrations of released P accompanied by Fe(III) in iron(III) phosphates reduction were determined after treatment with molybdenum blue color reagents according to the obtained standard curve. All experiments were performed in at least three replicates at 25 °C.

***In Situ* AFM Imaging for Surface Dissolution of Iron(III) Phosphates.** *In situ* surface dissolution experiments of AmFe(III)-P and CryFe(III)-P was examined with an AFM instrument (Nanoscope Multimode 8, Bruker) equipped with a 100 μL liquid cell allowed for various biogeochemical reactions. AFM images were obtained using commercially available Si_3N_4 probes (Bruker ScanAsyst Fluid+, $k = 0.7$ N/m and tip radius 2 nm) under ScanAsyst in Fluid model at a scan rate of 2.0 Hz for 2×2 μm^2 at 25 °C. Prior to the dissolution experiments, AmFe(III)-P or CryFe(III)-P minerals were pressed at 15-20 MPa for 5-10 min to form smooth substrates. The newly-prepared reaction solutions with redox-active H_2PHZ were flowed through the liquid cell by a high-precision syringe pump (Razel Scientific Instruments model R100-E) at a constant rate of 10 mL/h to ensure steady-state kinetic dissolution conditions rather than diffusion-controlled dissolution conditions during a period of dissolution experiments.[19] The determination of dissolution rates in different aqueous solutions were performed from surface dissolution volume calculated by the Nanoscope Analysis software with Bearing Analysis model. The obtained dissolution rates were all shown as mean values ± standard deviation of three independent sets. In addition, for reductive

dissolution-reprecipitation experiment, the 200 mg/L PCA-bearing solution with 2 mM KH_2PO_4 was pumped into the AFM system for *in situ* observation of the formation of amorphous Fe(II)-P (AmFe(II)-P) particles on AmFe(III)-P surface.

XRD, XPS and Raman Spectroscopy Experiments. The phase identification of synthesized AmFe(III)-P and CryFe(III)-P mineral was conducted by X-ray diffraction (XRD) with the scanning speed of 4°/min from 5-90° and Raman spectroscopy (Horiba LabRAM HR800) by a laser 532 nm with 50 μm confocal hole and a 600 lines/mm grating under a 50 x microscope objective (Olympus, MLPlanTL N). The spectra were collected twice and analyzed with the LabSpec 6 software. *In situ* Raman spectroscopy was also used to characterize the newly-formed particles on AmFe(III)-P surface. These newly-formed particles were ultrasonically isolated from iron(III) phosphate surfaces after washing for further characterization of phase and chemical valence with XRD and X-ray Photoelectron Spectroscopy (XPS), respectively, after washing with water and alcohol multiple times. The obtained XPS data were analyzed by the Thermal Advantage software with smart background methods for baseline correction and Gaussian function for peak fitting. All measurements were performed for least three times to ensure the reproducibility of results.

Kelvin Potential Force Microscopy (KPFM). Samples used for KPFM experiment were collected from AmFe(III)-P surface before and after treatment with a binary combination of 100 mg/L 1-OHPHZ and 100 mg/L alginate with different concentrations and polymerization degrees. The contact potential difference ($V_{CPD} = V_{sample} - V_{tip}$) between the sample surface and a conductive AFM tip (MESP-V2, k = 3.0 N/m and tip radius 35 nm with a resonance frequency of 75 kHz) was determined by an AFM-based KPFM technique. To determine the surface potential of AFM tips, we first used a gold surface (PFKPEM-SMPL, Bruker) with a defined gold work function (Φ_{Au}) of 5.10 eV[20] as a reference to calibrate the work function of AFM tips (Φ_{tip}), which can be obtained by the following equation:

$$V_{CPD} = \frac{1}{e}\left(\Phi_{tip} - \Phi_{Au}\right) \qquad (1)$$

In the KPFM model, the sample surface topography and contact potential could be

obtained simultaneously and independently through a two-pass procedure.[21] In the first pass, the topographic image of sample surface was captured in AFM-based Tapping mode, and then the AC (V_{AC}) and DC (V_{DC}) voltage signals both were applied to the probe tips for nullifying the electrostatic interaction through a feedback loop using the following equation:

$$V_{tip} = \Delta V_{DC} + V_{AC} \sin(\omega t) \tag{2}$$

, where V_{AC} is induced by electrostatic interaction between probe tip and sample surface arising from a cantilever oscillation with an oscillating electric force on the cantilever at the resonant frequency of ω while lifting tips above sample surface. At the same time, we noted that in the lift mode, the cantilever vibration occurred with a detectable amplitude and moreover, the feedback loop adjusted the V_{DC} difference between probe tips and sample surfaces to maintain the physical oscillation amplitude of cantilever at zero ($\triangle V_{DC} = 0$).[22] As a result, the cantilever oscillation and the electric force applied onto cantilever were disappeared simultaneously.[22] And in this way, V_{DC} applied to probe tip was equal to V_{CPD}[21-23] and was recorded through constructing a voltage map of sample surface. Considering that the drift of sample surface potential, the sample surface potential should be collected after each 30 min scanning time to ensure data stability and accuracy. The surface potential was quantitatively determined in at least three independence-treated samples and a minimum of three different locations of each treatment. All values derived from V_{CPD} were shown as mean value ± standard deviation.

Table S1. Reductive dissolution rate ($\times 10^6$ nm^3 per 4 μm^2·min) of AmFe(III)-P and CryFe(III)-P by H$_2$PHZ (200 mg/L 1-OHPHZ, PCA or PCN) in a solution condition of pH 5 and high salt.

Fe(III)-P	Dissolution rate ($\times 10^6$ nm^3 per 4 μm^2·min)		
	1-OHPHZ	PCA	PCN
Amorphous	0.48 ± 0.05	0.31 ± 0.03	0.19 ± 0.01
Crystalline	0.27 ± 0.02	0.07 ± 0.01	0.04 ± 0.005

Table S2. Reductive dissolution rate ($\times 10^6$ nm^3 per 4 μm^2·min) of AmFe(III)-P and CryFe(III)-P by PCA in a high salt solution condition with different pH values (4, 5, 7 and 8).

Fe(III)-P	Dissolution rate ($\times 10^6$ nm^3 per 4 μm^2·min)			
	PCA in different pH values (High salt)			
	4	5	7	8
Amorphous	0.43 ± 0.06	0.31 ± 0.03	0.17 ± 0.02	0.10 ± 0.01
Crystalline	0.15 ± 0.02	0.07 ± 0.01	0.05 ± 0.008	0.03 ± 0.002

Table S3. Reductive dissolution rate ($\times 10^6$ nm^3 per 4 μm^2·min) of AmFe(III)-P and CryFe(III)-P by PCA in a low salt solution condition with different pH values (4, 5, 7 and 8).

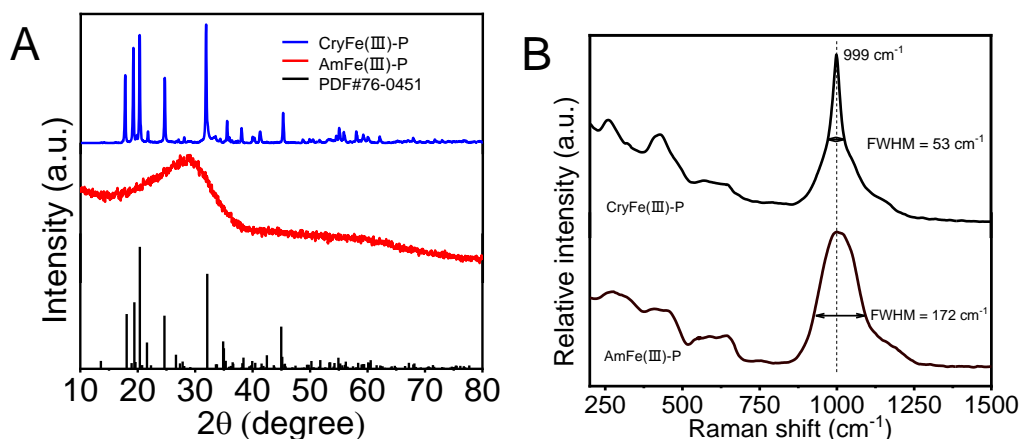| Fe(III)-P	Dissolution rate ($\times 10^6$ nm^3 per 4 μm^2·min)			
	PCA in different pH values (Low salt)			
	4	5	7	8
Amorphous	0.28 ± 0.04	0.21 ± 0.02	0.07 ± 0.009	0.06 ± 0.005
Crystalline	0.10 ± 0.008	0.04 ± 0.005	0.03 ± 0.004	0.01 ± 0.002

Figure S1. Identifications of synthesized AmFe(III)-P and CryFe(III)-P by (A) XRD and (B) Raman spectroscopy, respectively.
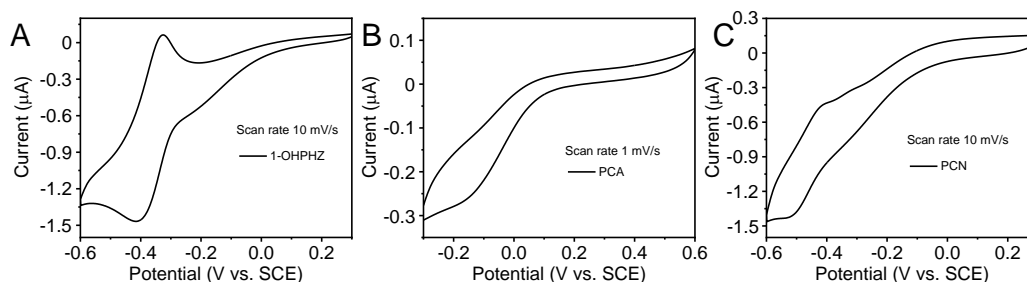

Figure S2. Cyclic voltammetry (CV) results of (A) 1-OHPHZ, (B) PCA and (C) PCN collectively exhibit single oxidation and reduction peaks in solution conditions (pH 7; high salt) buffered with 10 mM $CH_3C(O)ONH_4$-MOPS (5 mM each).
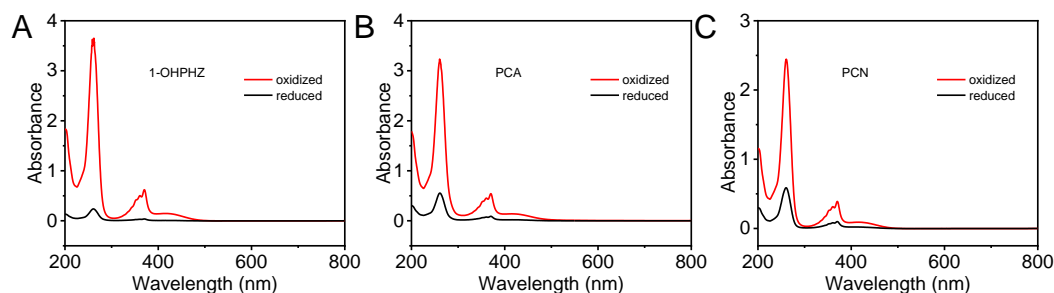

Figure S3. Characteristic UV-visible spectra for the oxidized and reduced couples of (A) 1-OHPHZ, (B) PCA and (C) PCN in a buffer solution with pH 7 and high salt.
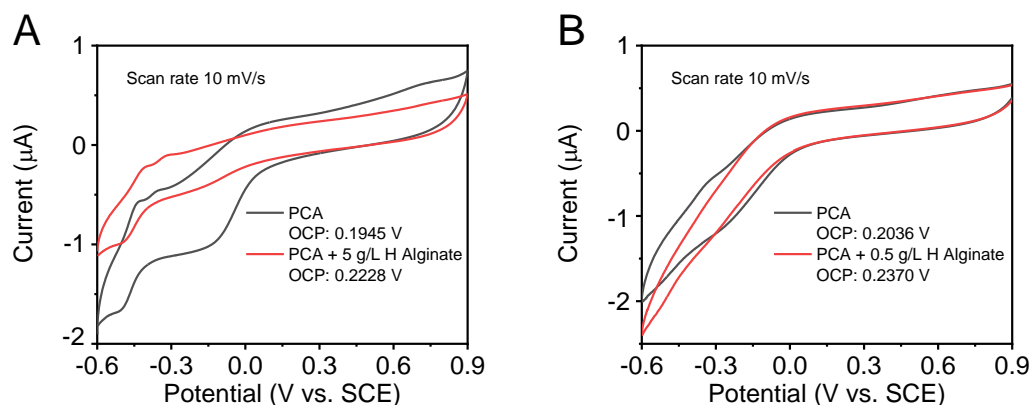
Figure S4. CV curves of PCA before and after treatment with (A) 5 g/L and (B) 500 mg/L H alginate at scan rate of 10 mV/s in a buffer solution with pH 7 and high salt. The open circuit potential (OCP) values of reduced PCA before and after treatment with H alginate are shown in (A) and (B).
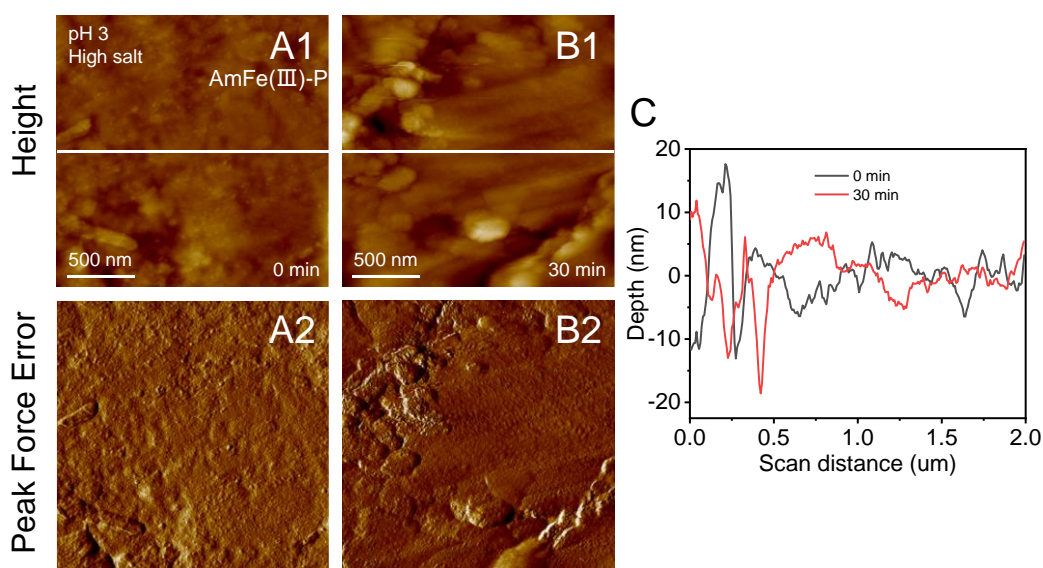

Figure S5. AFM height images of surface dissolution of AmFe(III)-P at (A1) 0 min and (B1) 30 min, and corresponding peak force error images at (A2) 0 min and (B2) 30 min, respectively. Height profiles of AmFe(III)-P mineral surface along the white lines are shown in (C).
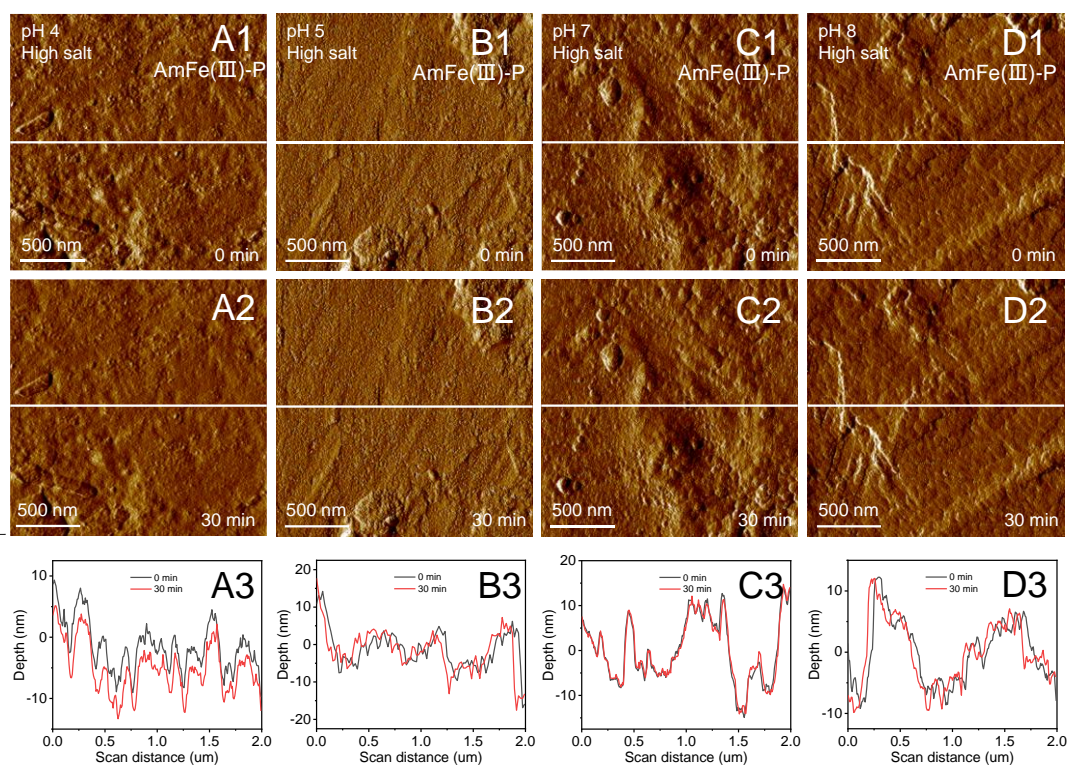
Figure S6. AFM peak force error images of surface dissolution of AmFe(III)-P with time after exposure to a high salt buffer solution without H_2PHZ at (A1-A2) pH 4, (B1-B2) pH 5, (C1-C2) pH 7, (D1-D2) pH 8, respectively. Height profiles of AmFe(III)-P surface along the white lines in both 0 and 30 min are shown in (A3-D3), illustrated the unchanged surface morphologies at the nanoscale during the process.
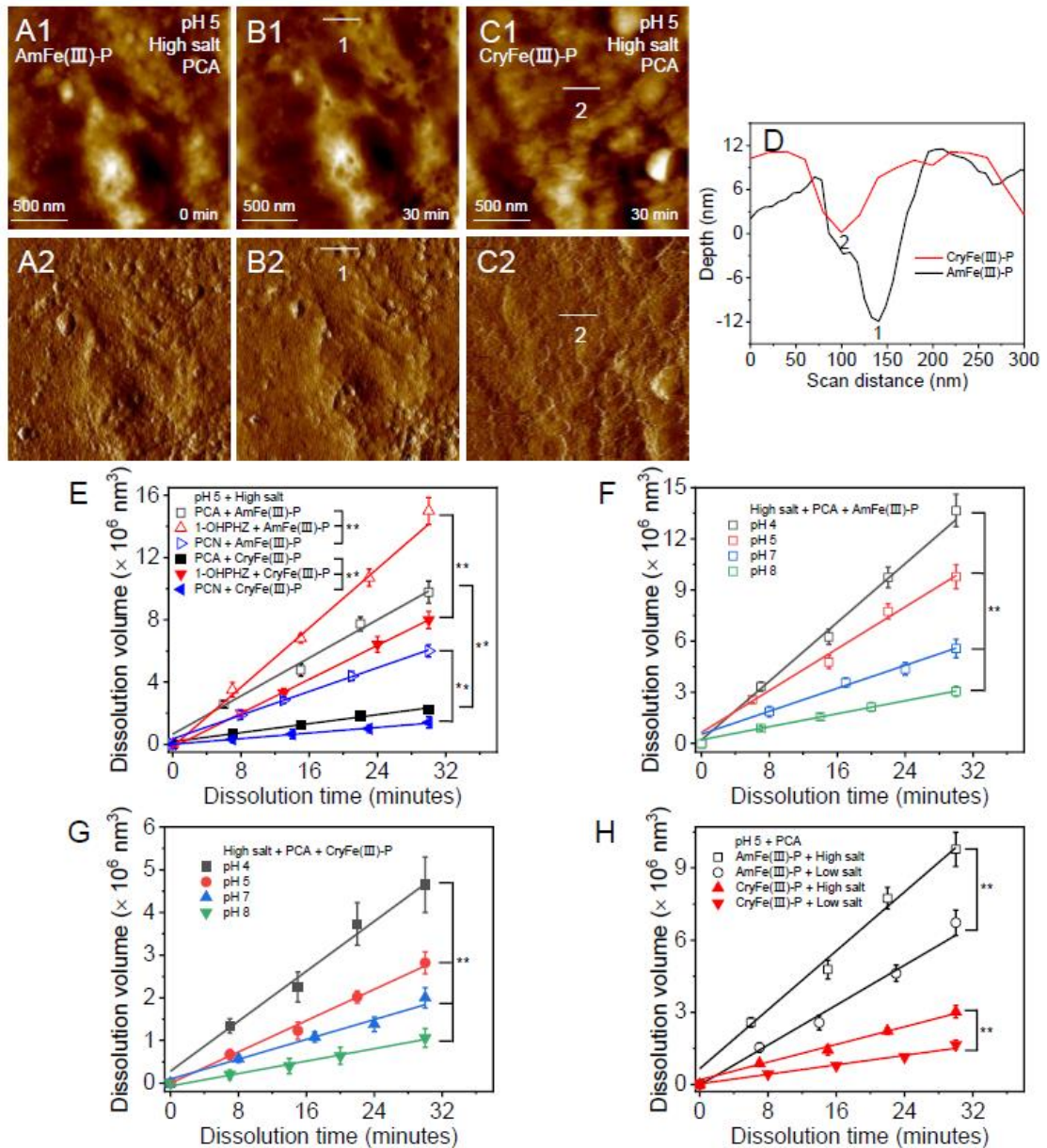
Figure S7. *In situ* AFM height images of a representative reductive dissolution event on the surfaces of (A1-B1) AmFe(III)-P and (C1) CryFe(III)-P minerals and corresponding deflection images on the surfaces of (A2-B2) AmFe(III)-P and (C2) CryFe(III)-P minerals with time after exposure to a 200 mg/L PCA-bearing buffer solution (pH 5; high salt). Height profiles of etch pits along the white lines 1 and 2 are shown in (D), illustrating the deeper etch pit depth on AmFe(III)-P surface than that on CryFe(III)-P surface after treatment with the same reaction solution and time. The reductive dissolution volume increases linearly with time after exposure to (E) different H₂PHZ-bearing buffer solutions (200 mg/L; pH 5; high salt) on the surfaces of

AmFe(III)-P and CryFe(III)-P; or after exposure to a 200 mg/L PCA-bearing buffer solution with high salt on surfaces of (F) AmFe(III)-P and (G) CryFe(III)-P, respectively, at four pH values (4, 5, 7 and 8); or after exposure to a 200 mg/L PCA-bearing buffer solution with pH 5 on AmFe(III)-P and CryFe(III)-P surfaces at (H) different salt concentrations (high salt; low salt), respectively.
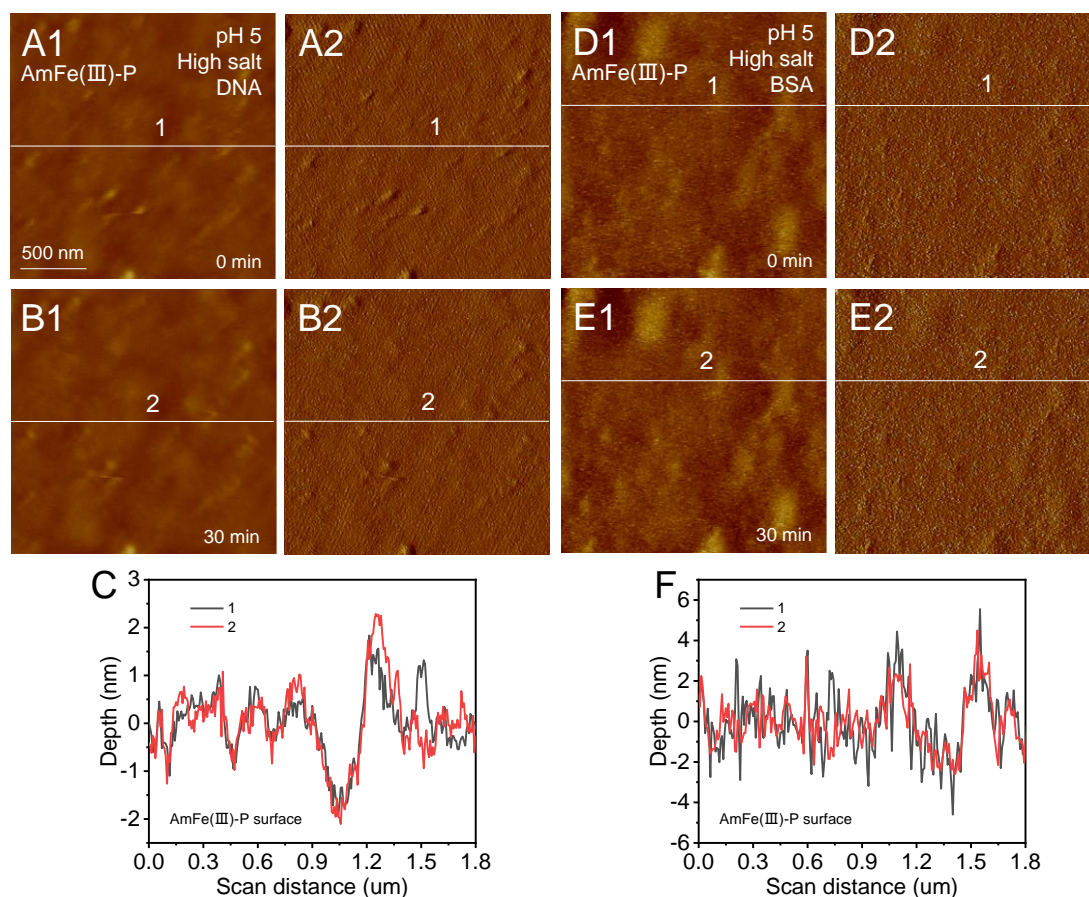

Figure S8. *In situ* AFM height images of a representative surface morphology of AmFe(III)-P and corresponding deflection images of AmFe(III)-P with time after exposure to (A2-B2) a 200 mg/L eDNA-bearing or (D1-E1) a 200 mg/L BSA-bearing solution (pH 5; high salt), respectively. Height profiles of etch pits along the white lines 1 and 2 are shown in (C) and (F), illustrating the unchanged height of morphologies on AmFe(III)-P surface after treatment with the same reaction solution and time.
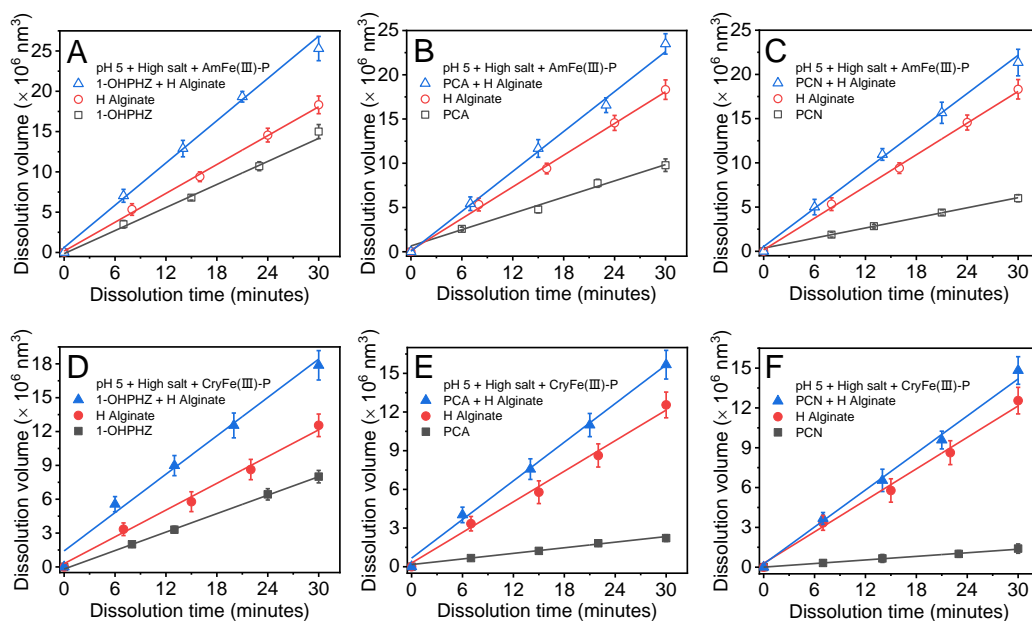
Figure S9. The dissolution volume increases linearly with time; slopes of lines and the dissolution rates follow the order: H_2PHZ + H alginate > H alginate > H_2PHZ whether on the surfaces of (A-C) AmFe(III)-P or (D-F) CryFe(III)-P mineral with respect to solution conditions of pH 5 and high salt.
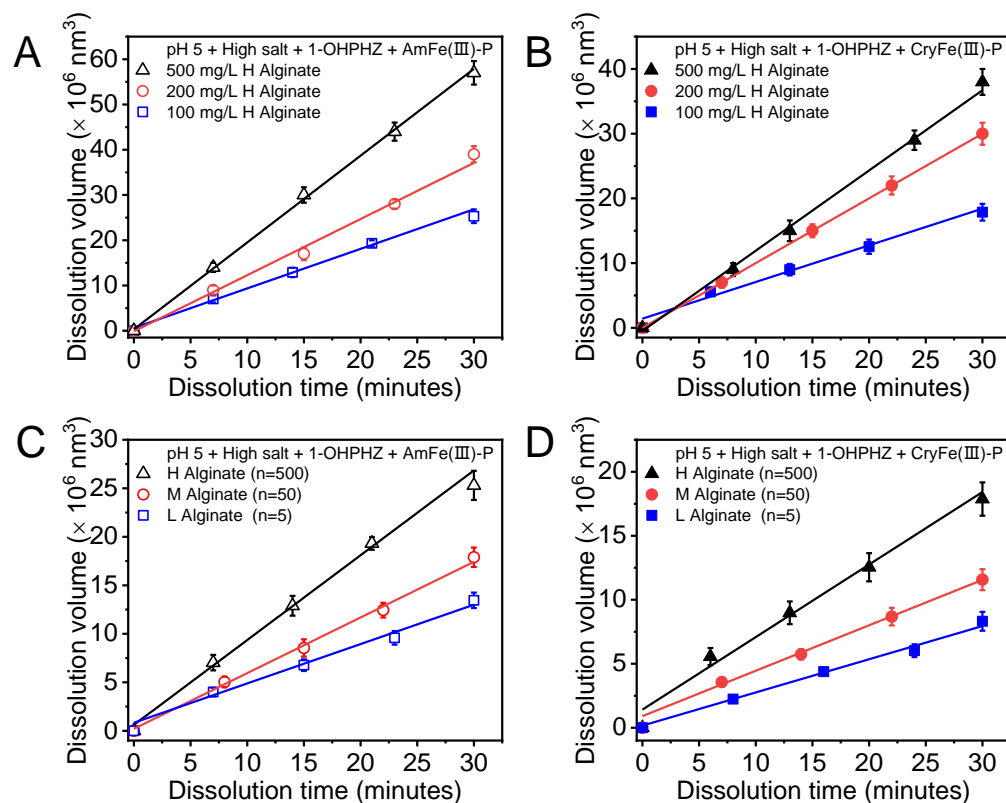
Figure S10. The dissolution volume increases linearly with time after exposure to a 100 mg/L 1-OHPHZ-bearing buffer solution (pH 5; high salt) with (A-B) different concentrations of H alginate (100, 200 and 500 mg/L) or (C-D) different degrees of polymerization of 100 mg/L alginate (H, M and L) on surfaces of AmFe(III)-P and CryFe(III)-P, respectively.
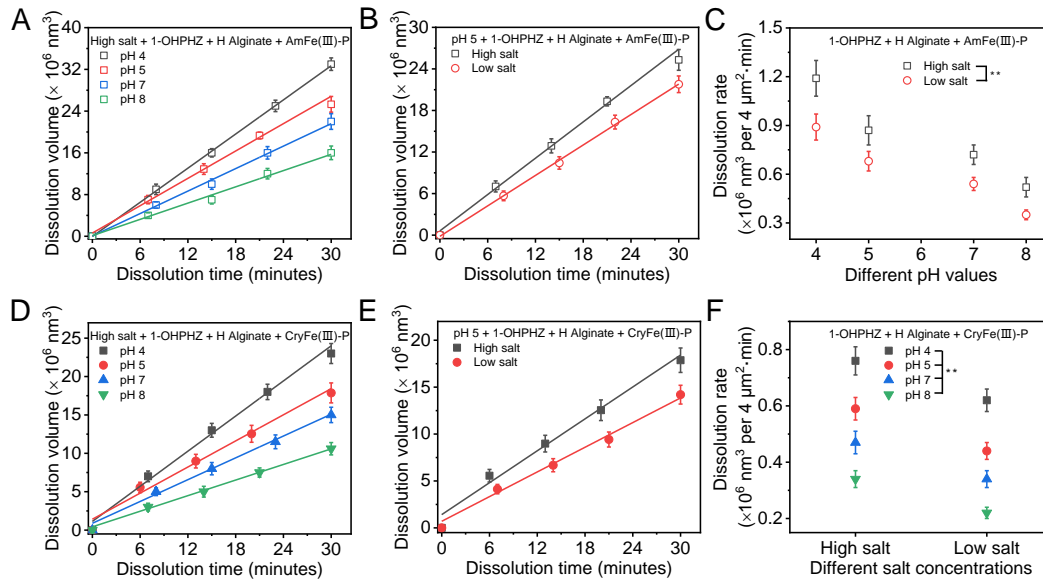

Figure S11. The dissolution volume increases linearly with time after exposure to a 200 mg/L 1-OHPHZ-bearing buffer solution on AmFe(III)-P and CryFe(III)-P surfaces at (A, D) four pH values (4, 5, 7 and 8) with high salt and (B, E) different salt concentrations (high salt, low salt) with pH 5, respectively. Significant analyses of dissolution rates after exposure to a 200 mg/L 1-OHPHZ-bearing buffer solution at four pH values (4, 5, 7 and 8) with different salt concentrations (high and low salt) in the presence of (C) AmFe(III)-P and (F) CryFe(III)-P of 100 mg, respectively. The error bars represent standard deviations taken from independent triplicate experiments. Two asterisks indicate significant differences at $P < 0.01$, which was analyzed by SPSS software.

Figure S12. Total Fe and P production in a 200 mg/L 1-OHPHZ-bearing buffer solution at four pH values (4, 5, 7 and 8) with different salt concentrations (high salt, low salt) in the presence of 100 mg (A-B) CryFe(III)-P or (C) AmFe(III)-P, respectively. The error bars represent standard deviations taken from independent triplicate experiments. Two asterisks indicate significant differences at $P < 0.01$, which was analyzed by SPSS software.
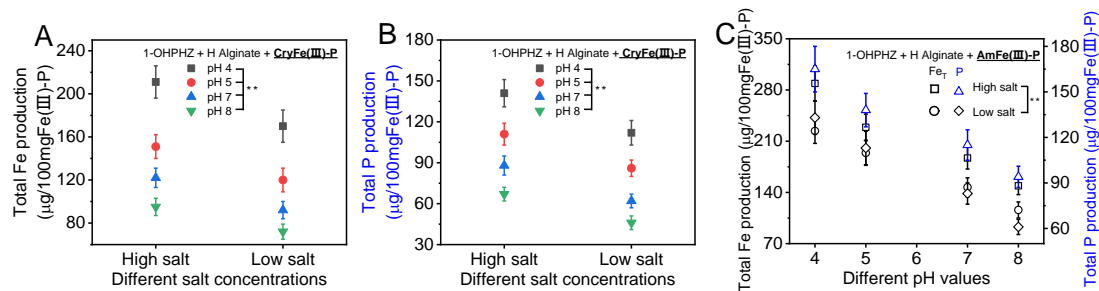
References

(1) J. Baumgartner, G. Morin, N. Menguy, T. Perez Gonzalez, M. Widdrat, J. Cosmidis and D. Faivre, Magnetotactic bacteria form magnetite from a phosphate-rich ferric hydroxide via nanometric ferric (oxyhydr)oxide intermediates, *Proc. Natl. Acad. Sci. U. S. A.*, 2013, **110**, 14883–14888.

(2) J. Cosmidis, K. Benzerara, G. Morin, V. Busigny, O. Lebeau, D. Jézéquel, V. Noël, G. Dublet and G. Othmane, Biomineralization of iron-phosphates in the water column of Lake Pavin (Massif Central, France). *Geochim. Cosmochim. Acta,* 2014, **126**, 78–96.

(3) M. Seder-Colomina, G. Morin, J. Brest, G. Ona-Nguema, N. Gordien, J. Pernelle, D. Banerjee, O. Mathon, G. Esposito and E. D. van Hullebusch, Uranium(VI) scavenging by amorphous iron phosphate encrusting sphaerotilus natans filaments, *Environ. Sci. Technol.*, 2015, **49**, 14065−14075.

(4) Y. Li, Y. Li, K. Zhang, R. Xu, M. Yuan and Y. Yao, Influence of synthesis parameters on the properties of $FePO_4 \cdot 2H_2O$ used for the precursor of $LiFePO_4$ cathode material, *Ionics,* 2021, **27**, 983-991.

(5) Y. Wang and D. K. Newman, Redox reactions of phenazine antibiotics with ferric (hydr)oxides and molecular oxygen, *Environ. Sci. Technol.*, 2008, **42**, 2380–2386.

(6) L. L. Stookey, Ferrozine: A new spectrophotometric reagent for iron, *Anal. Chem.*, 1970, **42**, 779−781.

(7) M. J. Pullin and S. E. Cabaniss, The effects of pH, ionic strength, and iron-fulvic acid interactions on the kinetics of non-photochemical iron transformations. I. Iron(II) oxidation and iron(III) colloid formation, *Geochim. Cosmochim. Acta,* 2003, **67**, 4067−4077.

(8) A. N. Pham and T. D. Waite, Oxygenation of Fe(II) in the presence of citrate in aqueous solutions at pH 6.0−8.0 and 25 °C: Interpretation from an Fe(II)/citrate speciation perspective, *J. Phys. Chem. A,* 2008, **112**, 643−651.

(9) J. C. Thompsen and H. A. Mottola, Kinetics of the complexation of iron(II) with ferrozine, *Anal. Chem.*, 1984, **56**, 755−757.

(10) J. Lin and D. R. Kester, The kinetics of Fe(II) complexation by ferrozine in seawater, *Mar. Chem.*, 1992, **38**, 283−301.

(11) E. E. Daugherty, B. Gilbert, P. S. Nico and T. Borch, Complexation and redox buffering of iron(II) by dissolving organic matter, *Environ. Sci. Technol.*, 2017, **51**, 11096-11104.

(12) H. Wang, H. Yao, P. Sun, D. Li and C. Huang, Transformation of tetracycline antibiotics and Fe and Fe species induced by their complexation, *Environ. Sci. Technol.*, 2016, **50**, 145-153.

(13) E. Voillier, P. W. Inglett, K. Hunter, A. N. Roychoudhury and P. Van Cappellen, The ferrozine method revisited: Fe(II)/Fe(III) determination in natural waters, *Appl. Geochem.*, 2000, **15**, 785–790.

(14) K. Amstaetter, T. Borch and A. Kappler, Influence of humic acid imposed changes of ferrihydrite aggregation on microbial Fe(II) reduction, *Geochim. Cosmochim. Acta,* 2012, **85**, 326-341.

(15) S. Garg, C. Jiang and T. D. Waite, Impact of pH on iron redox transformation in simulated freshwaters containing natural organic matter, *Environ. Sci. Technol.*, 2018, **52**, 13184−13194.

(16) E. C. Maters, P. Delmelle and S. Bonneville, Atmospheric processing of volcanic

glass: effects on iron solubility and redox speciation, *Environ. Sci. Technol*., 2016, **50**, 5033−5040.

(17) L. Zhang, Y. Chen, Q. Xia, K. M. Kemner, Y. Shen, E. J. O'Loughlin, Z. Pan, Q. Wang, Y. Huang, H. Dong and M. I. Boyanov, Combined effects of Fe(III)-bearing clay minerals and organic ligands on U(VI) bioreduction and U(IV) speciation. *Environ. Sci. Technol*., 2021, **55**, 5929−5938.

(18) J. Murphy and J. P. Riley, A modified single solution method for the determination of phosphate in natural waters. *Anal. Chim. Acta,* 1962, **27**, 31-36.

(19) X. Ge, L. Wang, W. Zhang and C. V. Putnis, Molecular understanding of humic Acid-limited phosphate precipitation and transformation. *Environ. Sci. Technol*., 2020, **54**, 207−215.

(20) S. Trasatti, Operative (electrochemical) work function of gold. *J. Electroanal. Chem, Interfacial Electrochem*., 1974, **54**, 19–24.

(21) C. Leung, H. Kinns, B. W. Hoogenboom, S. Howorka and P. Mesquida, Imaging Surface Charges of Individual Biomolecules, *Nano Lett*., 2009, **9**, 2769−2773.

(22) M. Fujihira, Kelvin Probe Force Microscopy of Molecular Surfaces, *Annu. Rev. Mater. Sci*., 1999, **29**, 353−380.

(23) C. C. Tsai, H. H. Hung, C. P. Liu, Y. T. Chen and C. Y. Pan, Changes in plasma membrane surface potential of PC12 cells as measured by kelvin probe force microscopy, *PLoS One,* 2012, **7**, e33849.